Inorganica Chimica Acta 406 (2013) 160–170

Contents lists available at ScienceDirect

Inorganica Chimica Acta

journal homepage: www.elsevier.com/locate/ica

Syntheses, spectroscopic properties, crystal structures, biological activities, and DNA interactions of heterocyclic amine substituted *spiro-ansa-spiro*- and *spiro-bino-spiro*-phosphazenes

Selen Bilge Koçak [a,*], Serhat Koçoğlu [a], Aytuğ Okumuş [a], Zeynel Kılıç [a], Aslı Öztürk [b], Tuncer Hökelek [b], Yağmur Öner [c], Leyla Açık [c]

[a] Department of Chemistry, Ankara University, 06100 Tandoğan-Ankara, Turkey
[b] Department of Physics, Hacettepe University, 06800 Beytepe-Ankara, Turkey
[c] Department of Biology, Gazi University, 06500 Beşevler-Ankara, Turkey

ARTICLE INFO

Article history:
Received 17 January 2013
Received in revised form 21 June 2013
Accepted 14 July 2013
Available online 22 July 2013

Keywords:
Spiro-ansa-spiro-phosphazenes
Spiro-bino-spiro-phosphazenes
Spectroscopy
Crystal structure
DNA interactions

ABSTRACT

The heterocyclic amine e.g. pyrrolidine, piperidine, morpholine and 1,4-dioxa-8-azaspiro[4,5]decane (DASD) substituted *spiro-ansa-spiro* (**sas**) **5a–5d** and *spiro-bino-spiro* (**sbs**) **6a–6d** phosphazenes were prepared by the replacement reactions of the Cl-atoms in **3** and **4** with heterocyclic amines in dry THF (Scheme 1). All of the phosphazene derivatives were characterized by elemental analysis, FTIR, MS, 1D ^{1}H, ^{13}C and ^{31}P NMR and DEPT and 2D HSQC techniques. The crystal structures of fully morpholine substituted **sas 5c** and **sbs 6c** phosphazenes were verified by X-ray diffraction analysis. The relationships between exocyclic OPN bond angles (α') and δP_{OPN} shifts, and the correlation of Δ(P–N) values and $\Delta(\delta P)$ or δP_{OPN} shifts were presented. The phosphazene derivatives (**3**, **4**, **5a–5d** and **6a–6d**) were subjected to antimicrobial activity against six pathojen bacteria and two yeast strains. Fully pyrrolidine substituted **sbs 6a** was found to be quite active against yeast strain *Candida tropicalis*. In addition, the nature of the interactions of these compounds with pBR322 plasmid DNA was investigated, and the results displayed that partly substituted **sas 3** and **sbs 4** caused to cleave the DNA.

1. Introduction

Cyclophosphazenes are versatile inorganic ring systems composed of a backbone that contains the repeating unit $[NPR_2]_n$ (n = 3, 4, 5, ...) with trivalent nitrogen and pentavalent phosphorus atoms and two organic, inorganic and organometallic side groups (R), covalently linked to each phosphorus atom [1]. They have diverse applications as hydraulic fluids or lubricants [2], ionic liquids [3], liquid crystalline materials [4], flame retardant additives to organic polymers [5], light-emitting diodes [6], electrolytes for lithium-ion batteries [7], and monomers for inorganic high molecular weight polymers [8]. The hexachlorocyclotriphosphazene (cyclic trimer, $N_3P_3Cl_6$) has served as an important starting compound in the field of phosphazene chemistry. One to all six Cl-atoms in $N_3P_3Cl_6$ can be substituted by the same or different groups. Therefore, there is no limit for the number of PN/substituent combinations. A wide range of cyclotriphosphazene derivatives with different side groups and with diverse application potential has been prepared using the replacement of highly reactive Cl-atoms at P-atoms in $N_3P_3Cl_6$ by a variety of –NH or –OH functionalized nucleophilic reagents, such as primary [9] and secondary [10] amines, polyamines [11] and phenols [12]. Among these, the substitution reactions of $N_3P_3Cl_6$ with difunctional nucleophiles have received a lot of attention in recent two decades due to the formation of numerous structural isomers and stereoisomers. The reactions involving difunctional reagents with $N_3P_3Cl_6$ have been found to proceed *via* different routes. The interactions of one of the Cl-atoms with one functional group of the nucleophile give open-chain dangling precursors [13]. The replacement of two geminal and two non-geminal Cl-atoms yields *spiro*- and *ansa*-substituted isomeric products, respectively [14]. The intermolecular reactions between the heterofunctional dangling precursor with a Cl-atom of the next molecule of $N_3P_3Cl_6$ produce *bino*-architecture composed of two chlorocyclotriphosphazene moieties bridged with the respective difunctional reagent [15]. In general, the nature of the products formed in these reactions is controlled by a variety of factors such as the chain lengths of the reacting functional groups, reaction temperature and the solvent polarities [16]. The number of *spiro-ansa*-, *spiro-bino*- or *ansa-bino*-phosphazene derivatives has been relatively limited in the literature [17–19]. On the other hand, some of the cycloptrihosphazene derivatives substituted heterocyclic amines such as aziridine, pyrrolidine and morpholine have revealed significant antimicrobial and antitumor

* Corresponding author. Tel.: +90 312 2126720 1021; fax: +90 312 2232395.
E-mail address: sbilge@science.ankara.edu.tr (S. Bilge Koçak).

0020-1693/$ - see front matter © 2013 Elsevier B.V. All rights reserved.
http://dx.doi.org/10.1016/j.ica.2013.07.023

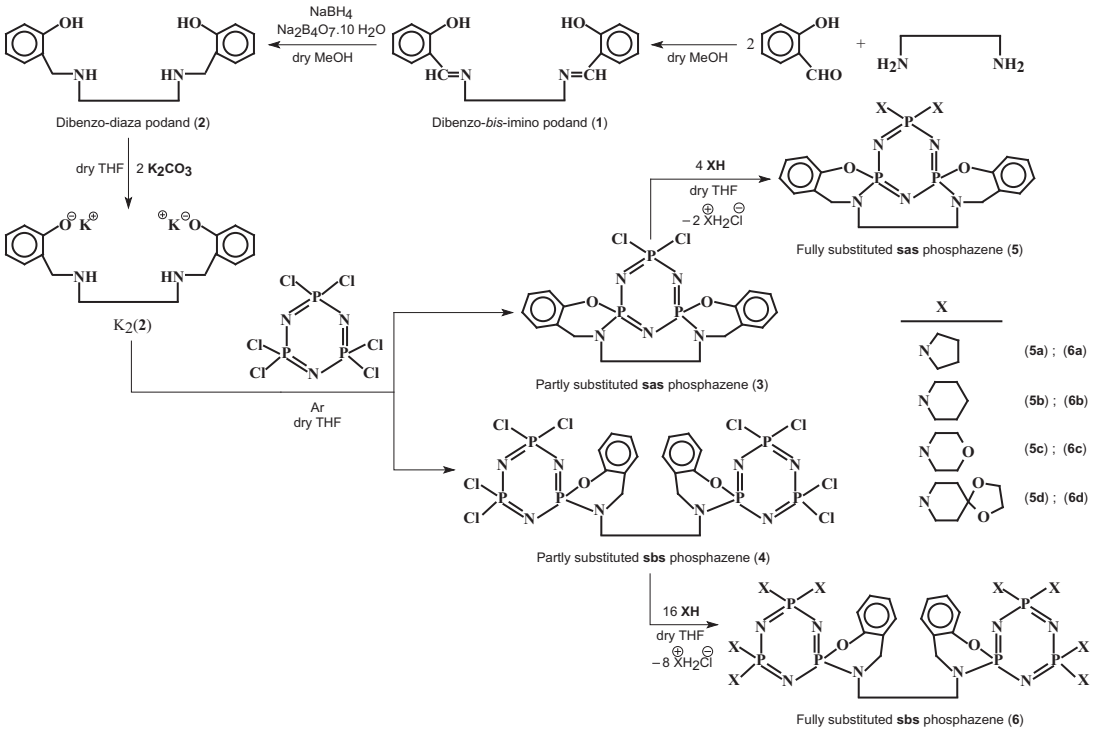

Scheme 1. The phosphazene derivatives obtained from the reactions of $N_3P_3Cl_6$ with dibenzo- diaza podand, pyrrolidine, piperidine, morpholine and DASD.

activities and have been effective in changing the mobility of the DNA [20–22]. Thus, it has been decided to introduce heterocyclic amine groups to the partly substituted **sas 3** and **sbs 4** phosphazenes with the aim of the investigations of their antimicrobial activities and DNA interactions.

The present paper reports herein: (i) The synthesis of fully heterocyclic amine substituted **sas 5a–5d** and **sbs 6a–6d** phosphazenes (Scheme 1), (ii) The structure determinations of eight new cyclotriphosphazene derivatives (**5b**, **5c** and **6a–6d**) by elemental analysis; mass spectrometry (MS); fourier transform infrared (FTIR); one-dimensional (1D) ^{1}H, ^{13}C and ^{31}P NMR; distortionless enhancement by polarization transfer (DEPT), and two-dimensional (2D) heteronuclear single quantum correlation (HSQC) techniques, (iii) The solid-state and molecular structures of fully morpholine substituted **sas 5c** and **sbs 6c** phosphazenes, (iv) The relationship between the δP_{OPN} shifts and the exocyclic OPN bond angles (α'), and the correlation of Δ(P–N) values and $\Delta(\delta P)$ chemical shift differences or δP_{OPN} shifts, (v) The investigations of antibacterial and antifungal activities of **3**, **4**, **5a–5d** and **6a–6d**, and (vi) Interactions between all of the **sas** and **sbs** compounds and pBR322 plasmid DNA.

2. Experimental

2.1. Materials used for synthesis

The solvents, salicylaldehyde, sodium borohydride, borax, potassium carbonate, piperidine and morpholine were purchased from Merck. Hexachlorocyclotriphosphazene, $N_3P_3Cl_6$ (Fluka), was purified by fractional crystallization from *n*-hexane. 1,2-Diaminoethane, pyrrolidine and DASD were obtained from Fluka. All reactions were monitored using thin-layer chromatography (TLC) on Merck DC Alufolien Kiesegel 60 B_{254} sheets. Column chromatography was performed on Merck Kiesegel 60 (230–400 mesh ATSM) silica gel.

2.2. Physical measurements

Melting points were measured with a Gallenkamp apparatus using a capillary tube. Microanalyses (C, H, N) were performed using Leco CHNS-932 elemental analyzer by the Central Instrumental Analysis Lab., Faculty of Pharmacy, Ankara University. ^{1}H (400 MHz) and ^{13}C (100 MHz) NMR, DEPT and HSQC spectra were recorded employing a Varian Mercury 400 MHz FT spectrometer, and ^{31}P NMR spectra were obtained Bruker DPX FT-NMR 500 MHz spectrometer ($SiMe_4$ was used as an internal standard for ^{1}H and ^{13}C NMR, and external 85% H_3PO_4 for ^{31}P NMR). IR spectra were recorded on a Mattson 1000 FTIR spectrometer using KBr pellets. ESI-MS and API-ES mass spectra were obtained on the Agilent 1100 MSD spectrometer and Waters Micromass ZQ mass spectrometer, respectively.

2.3. Single crystal X-ray structure determination

The detailed crystallographic data and structure refinement parameters were summarized in Table 1 [23,24]. Selected bond lengths and angles for fully morpholine substituted **sas 5c** and **sbs 6c** phosphazenes are given in Table 1S. Crystallographic data were recorded on an Enraf–Nonius CAD-4 (for **5c**) and Bruker Kappa APEXII (for **6c**) diffractometers using Mo Kα radiation (λ = 0.71073 Å) at T = 294 K (for **5c**) and T = 100(2) K (for **6c**). Absorption corrections by psi-scan [25] (for **5c**) and multi-scan [26] (for **6c**) were applied. Structures were solved by direct methods and refined by full-matrix least squares against F^2 using all data [27]. All non-H atoms were refined anisotropically. Aromatic, methylene and methyl H atoms were positioned geometrically at distances of 0.93 (CH), 0.97 (CH_2) and 0.96 (CH_3) (for **5c**) and 0.95 (CH), 0.99 (CH_2) and 0.98 (CH_3) (for **6c**) from the parent C atoms; a riding model was used during the refinement process and the U_{iso}(H) values were constrained to be 1.2 U_{eq} (for methine and methylene carrier atoms) and 1.5 U_{eq} (for methyl carrier atoms).

Table 1
Crystallographic data for **5c** and **6c**.

	(**5c**)	(**6c**)[a]
Empirical formula	$C_{24}H_{32}N_7O_4P_3{\cdot}C_2H_3N$	$C_{48}H_{80}N_{16}O_{10}P_6{\cdot}2C_2H_3N$
Color/shape	Colorless/rod-shaped	Colorless/block
Formula weight	616.53	1309.21
T (K)	298(2)	100(2)
Radiation used, graphite monochromator	Mo Kα (λ = 0.71073 Å)	Mo Kα (λ = 0.71073 Å)
Crystal system	$P2_1/a$	$P2_1/c$
Space group	monoclinic	monoclinic
a (Å)	15.5465(18)	15.8439(6)
b (Å)	11.0971(17)	10.0433(4)
c (Å)	18.2722(17)	21.0252(7)
α (°)	90.00	90.00
β (°)	109.954(8)	107.223(2)
γ (°)	90.00	90.00
V (Å^3)	2963.1(6)	3195.6(2)
Z	4	2
Absorption coefficient (mm^{-1})	0.248	0.237
D_{calc} (Mg m^{-3})	1.382	1.361
Maximum crystal dimension (mm)	0.25 × 0.30 × 0.35	0.32 × 0.38 × 0.48
θ_{max} (°)	26.29	28.44
Reflections measured	5999	5605
Range of h, k, l	$-19 < h < 0$, $0 < k < 13$, $-21 < l < 22$	$-17 < h < 18$, $-11 < k < 11$, $-25 < l < 25$
Diffractometer/scan	Enraf–Nonius Turbo CAD-4/non-profiled w	Bruker-Kappa APEXII CCD/ profiled φ and w
Number of reflections with $I > 2\sigma(I)$	4739	4921
Corrections applied	lorentz-polarization	lorentz-polarization
Computer programs	SHELXS97, SHELXL97, ORTEP-3	SHELXS97, SHELXL97, ORTEP-3
Source of atomic scattering factors	Int. Table for X-ray Cryst., vol. IV, 1974	Int. Table for X-ray Cryst., vol. IV, 1974
Structure solution	direct methods	direct methods
Treatment of hydrogen atoms	geometric calculations	geometric calculations
No. of parameters var.	372	389
Goodness-of-fit (GOF)	1.152	1.015
$R = \|\|F_o\| - \|F_c\|\|/\|F_o\|$	0.0562	0.0778
R_w	0.1459	0.2056
$(\Delta/\rho)_{max}$ (e A^{-3})	0.774	1.597
$(\Delta/\rho)_{min}$ (e A^{-3})	−0.746	−1.508

[a] The crystallographic data for **6c** do not sufficiently fulfill the requirements of the checkCIF program, but the data of **sbs 6c** were used in this study for comparison with the data (bond lengths and angles, hydrogen bondings, and conformation of the rings and Cremer–Pople parameters) of **sas 5c**.

2.4. Antibacterial activity

The agar well-diffusion method [28] was used to test the antimicrobial activities of the compounds against reference bacterial strains *Staphylococcus aureus* ATCC 25923 (G+), *Bacillus subtilis* ATCC 6633 (G+), *Bacillus cereus* NRRL-B-3711 (G+), *Enterococcus faecalis* ATCC 292112 (G+), *Pseudomonas aeruginosa* ATCC 27853 (G−), and *Escherichia coli* ATCC 25922 (G−). In addition, *Candida albicans* ATCC 10231 and*Candida tropicalis* ATCC 13803 were used for antifungal activities. Gram positive and gram negative bacteria were grown on Nutrient Broth agar plates and incubated at 37 °C for 24 h, and adjusted to a final concentration of 10^8 cfu/mL by diluting fresh cultures and compared to McFarland density. The yeast strains were grown in Sabouraud dextrose agar medium and incubated at 30 °C for 72 h. The medium was prepared, mixed with culture suspension, and poured into plates. The wells with a 6.0 mm diameter were made. The test compound was added to the well. After incubation, the diameter of inhibition zone was measured in millimeters. *Ampisilin* (10 μg/mL) and *Chloramphenicol* (30 μg/mL) were used as standard antibacterial agents. *Ketoconazole* (50 μg/mL) was used as an antifungal control. All the experiments were repeated three times.

2.5. DNA cleavage activity

The interactions between starting compound ($N_3P_3Cl_6$), pyrrolidine, morpholine, piperidine, DASD, dibenzo-diaza podand (**2**), **sas 3**, **5a**-**5d** and **sbs 4**, **6a**-**6d** phosphazenes and pBR322 plasmid DNA were studied by agarose gel electrophoresis [29]. These compounds were dissolved in DMSO. The solutions of the compounds were prepared and immediately applied to plasmid DNA. Plasmid DNA aliquots were incubated in the presence of increasing concentrations of the compounds ranging from 625 to 5000 μM at the 37 °C for 24 h. The aliquots of the compound-DNA mixtures (10 μL) were mixed with the buffer (0.1% bromophenol blue, 0.1% xylene cyanol) and loaded onto the 1% agarose gel. Electrophoresis was carried out under TAE (tris-acetate-EDTA) buffer for 3 h at 80 V. The gel was stained with ethidium bromide (0.5 μg/mL), viewed with a transilluminator (BioDoc Analyzer, Biometra), and the image was captured by a video-camera as a TIFF file.

2.6. Syntheses

Dibenzo-*bis*-imino-podand {N,N′-bis(salicylidene)-1,2-etanediamine} (**1**) and dibenzo-diaza-podand {bis[N,N'-(2-hydroxybenzyl)]1,2-diaminoetane} (**2**) were synthesized according to the published procedure [30]. The partly substituted **sas** phosphazene {8,8-dichloro-18,19-dihydro-6λ^5,8λ^5,10λ^5-6,10-nitrilo-16*H*,21*H*[1,3,5,7,2,4,6]tetrazatriphosphonino[2,1-b:6,7-b′]bis[1,3,2]benzoxazaphosphorine} (**3**) and **sbs** phosphazene {3,3′′-ethane-1,2-diylbis[4′,4′,6′,6′-tetrachloro-3,4-dihydrospiro[1,3,2-benzoxazaphosphorine-2,2′λ^5-[4λ^5,6λ^5][1,3,5,2,4,6]triazatriphosphorine]]} (**4**) were prepared using a method in which dibenzo-diaza-podand (**2**) and $N_3P_3Cl_6$ are refluxed in dry THF according to the published procedure by our research group [31]. Fully pyrrolidine and DASD substituted **sas** phosphazene derivatives {*meso*-18,19-dihydro-8,8-dipyrrolidine-1-yl-6λ^5,8λ^5,10λ^5-6,10-nitrilo-16*H*,21*H*[1,3,5,7,2,4,6]tetrazatriphosphecino[2,1-b:6,7-b′]bis[1,3,2]benzoxazaphosphorine} (**5a**) and {*meso*-18,19-dihydro-8,8-di(1,4-dioxa-8-azaspiro[4,5]decane)-1-yl-6λ^5,8λ^5,10λ^5-6,10-nitrilo-16*H*,21*H*[1,3,5,7,2,4,6]

tetrazatriphosphecino[2,1-b:6,7-b′]bis[1,3,2]benzoxazaphosphorine} (**5d**) were synthesized according to the our published procedure [32].

*2.6.1. Preparation of fully substituted **sas** phosphazenes (**5b** and **5c**)*

Compounds (**5b** and **5c**) were prepared by similar methods; therefore, the experimental procedure of the preparation is only described in detail for the first case.

*2.6.1.1. meso-18,19-Dihydro-8,8-dipiperidine-1-yl-6λ⁵,8λ⁵,10λ⁵-6,10-nitrilo-16H,21H[1,3,5,7,2,4,6]tetrazatriphosphecino[2,1-b:6,7-b′] bis[1,3,2]benzoxazaphosphorine (**5b**).* A solution of piperidine (0.72 g, 8.48 mmol) in 50 mL of dry THF was slowly added, over 0.5 h to a stirred solution of **3** (1.0 g, 2.10 mmol) in 200 mL of dry THF at ambient temperature with argon being passed over the reaction mixture. The mixture was stirred for 34 h at room temperature, and followed by TLC indicating no starting material remaining. The precipitated piperidine hydrochloride was filtered off, and the solvent was evaporated at reduced pressure. The crude product was subjected to column chromatography [silica gel 60 (70–230 mesh) (15 g) as adsorbent and toluene/THF (4/1) as the eluent] and crystallized from CH_3CN. Yield: 0.80 g (66%). mp: 218 °C. *Anal.* Calc. for $C_{26}H_{36}N_7O_2P_3$: C, 54.64; H, 6.35; N, 17.15. Found: C, 54.79; H, 6.28; N, 17.07%. IR (KBr, $\nu(cm^{-1})$): 3041 (C–H arom.), 2931–2829 (C–H aliph.), 1583 (C=C), 1184 (P=N). ESI-MS (I_r%): *m*/*z* 572 {[*M*H]$^+$, 92}.

*2.6.1.2. meso-18,19-Dihydro-8,8-dimorpholine-1-yl-6λ⁵,8λ⁵,10λ⁵-6,10-nitrilo-16H,21H[1,3,5,7,2,4,6]tetrazatriphosphecino[2,1-b:6,7-b′] bis[1,3,2]benzoxazaphosphorine (**5c**).* Compound (**5c**) was prepared from morpholine (0.37 g, 4.20 mmol) and **3** (0.5 g, 1.05 mmol) (36 h), column chromatography [silica gel (10 g), benzene/THF (1/1)], crystallized from CH_3CN. Yield: 0.45 g (70%). mp: 135 °C. *Anal.* Calc. for $C_{24}H_{32}N_7O_4P_3$: C, 50.09; H, 5.60; N, 17.04. Found: C, 50.16; H, 5.81; N, 16.97%. IR (KBr, $\nu(cm^{-1})$): 3071 (C–H arom.), 2960–2850 (C–H aliph.), 1585 (C=C), 1185 (P=N). API-ES (I_r%): *m*/*z* 576 {[*M*H]$^+$, 100}, 490 {[*M*-morpholine]$^+$, 3}.

*2.6.2. Preparation of fully substituted **sbs** phosphazenes (**6a**–**6d**)*

Compounds (**6a**–**6d**) were prepared by similar methods; therefore, the experimental procedure of the preparation is only described in detail for the first case.

*2.6.2.1. 3,3″-Ethane-1,2-diyllbis[3,4-dihydro-4′,4′,6′,6′-tetrapyrrolidine-1-yl(spiro[1,3,2-benzoxazaphosphorine-2,2′λ⁵-[4λ⁵,6λ⁵] [1,3,5,2,4,6]triazatriphosphorine]] (**6a**).* A solution of pyrrolidine (0.97 g, 13.6 mmol) in 50 mL of dry THF was slowly added, over 0.5 h to a stirred solution of **4** (0.7 g, 0.85 mmol) in 100 mL of dry THF at ambient temperature with argon being passed over the reaction mixture. The mixture was stirred for 65 h at room temperature, and followed by TLC indicating no starting material remaining. The precipitated pyrrolidine hydrochloride was filtered off, and the solvent was evaporated at reduced pressure. The crude product was subjected to column chromatography [silica gel 60 (70–230 mesh) (20 g) as adsorbent and toluene/THF (1/4) as the eluent] and crystallized from *n*-hexane. Yield: 0.69 g (74%). mp: 164 °C. *Anal.* Calc. for $C_{48}H_{80}N_{16}O_2P_6$: C, 52.50; H, 7.34; N, 20.39. Found: C, 52.73; H, 6.92; N, 19.80%. IR (KBr, $\nu(cm^{-1})$): 3043 (C–H arom.), 2960–2827 (C–H aliph.), 1587 (C=C), 1178 (P=N). API-ES (I_r%): *m*/*z* 1099 {[*M*H]$^+$, 100}, 547 {[*(pyrrolidine)$_4$P$_3$N$_3$OArCH$_2$NCH$_3$*]$^+$, 23}.

*2.6.2.2. 3,3″-Ethane-1,2-diyllbis[3,4-dihydro-4′,4′,6′,6′-tetrapiperidine-1-yl(spiro[1,3,2-benzoxazaphosphorine-2,2′λ⁵-[4λ⁵,6λ⁵] [1,3,5,2,4,6]triazatriphosphorine]] (**6b**).* Compound (**6b**) was prepared from piperidine (1.16 g, 13.6 mmol) and **4** (0.7 g, 0.85 mmol) (46 h), column chromatography [silica gel (10 g), benzene/THF (3/1)], crystallized from CH_3CN. Yield: 0.72 g (70%). mp: 232 °C. *Anal.* Calc. for $C_{56}H_{96}N_{16}O_2P_6$: C, 55.53; H, 7.99; N, 18.50. Found: C, 55.79; H, 7.51; N, 18.60%. IR (KBr, $\nu(cm^{-1})$): 3028 (C–H arom.), 2929–2817 (C–H aliph.), 1589 (C=C), 1180 (P=N). ESI-MS (I_r%): *m*/*z* 620 {[*(piperidine)$_4$P$_3$N$_3$OArCH$_2$NCH$_2$CH$_3$*]$^+$, 4}, 606 {[*(piperidine)$_4$P$_3$N$_3$OArCH$_2$NCH$_3$*]$^+$, 100}.

*2.6.2.3. 3,3″-Ethane-1,2-diyllbis[3,4-dihydro-4′,4′,6′,6′-tetramorpholine-1-yl(spiro[1,3,2-benzoxazaphosphorine-2,2′λ⁵-[4λ⁵,6λ⁵] [1,3,5,2,4,6]triazatriphosphorine]] (**6c**).* Compound (**6c**) was prepared from morpholine (1.18 g, 13.6 mmol) and **4** (0.7 g, 0.85 mmol) (60 h), column chromatography [silica gel (10 g), toluene/THF (1/1)], crystallized from CH_3CN. Yield: 0.64 g (69%). mp: >350 °C. *Anal.* Calc. for $C_{48}H_{80}N_{16}O_{10}P_6$: C, 46.98; H, 6.57; N, 18.26. Found: C, 46.66; H, 6.54; N, 17.74%. IR (KBr, $\nu(cm^{-1})$): 3055 (C–H arom.), 2958–2843 (C–H aliph.), 1589 (C=C), 1198 (P=N). API-ES (I_r%): *m*/*z* 1227 {[M*H*]$^+$, 43}, 614 {[*(morpholine)$_4$P$_3$N$_3$OArCH$_2$NCH$_3$*]$^+$, 12}.

*2.6.2.4. 3,3″-Ethane-1,2-diyllbis[3,4-dihydro-4′,4′,6′,6′-tetra(1,4-dioxa-8-azaspiro[4,5]decane)-1-yl(spiro[1,3,2-benzoxazaphosphorine-2,2′λ⁵-[4λ⁵,6λ⁵][1,3,5,2,4,6]triazatriphosphorine]] (**6d**).* Compound (**6d**) was prepared from DASD (1.95 g, 13.6 mmol) and **4** (0.7 g, 0.85 mmol) (60 h), column chromatography [silica gel (10 g), benzene/THF (1/1)], crystallized from CH_3CN. Yield: 1.02 g (72%). mp: >350 °C. *Anal.* Calc. for $C_{72}H_{112}N_{16}O_{18}P_6$: C, 51.61; H, 6.74; N, 13.37. Found: C, 51.50; H, 6.79; N, 13.27%. IR (KBr, $\nu(cm^{-1})$): 3030 (C–H arom.), 2956–2844 (C–H aliph.), 1591 (C=C), 1180 (P=N). ESI-MS (I_r%): *m*/*z* 838 {[*(DASD)$_4$P$_3$N$_3$OArCH$_2$NCH$_3$*]$^+$, 100}.

3. Results and discussion

3.1. Syntheses

The reaction of $N_3P_3Cl_6$ with K_2(**2**) was investigated by our group and two kinds of architectures, namely, *spiro-ansa-spiro* (**sas**) (**3**) and *spiro-bino-spiro* (**sbs**) (**4**) skeletons were obtained (Scheme 1). This reaction was carried out using two different ways of driving with or without triethylamine and different yields of **sas 3** and **sbs 4** phosphazenes were obtained. The yield of **sbs 3** (50%) was higher than that of **sas 4** (30%) in the absence of triethylamine and on a 1:2 M ratio reaction of $N_3P_3Cl_6$ and K_2(**2**). Whereas, the higher yield of **sas** (65%) and the lower yield of **sbs** (20%) were obtained in the presence of triethylamine as an HCl acceptor and in a 1:1 M ratio. This may be caused by the facilitate the nucleophilic attack of N–H nitrogen to P-atom with the formation of intermolecular hydrogen bonding involving triethylamine and N–H hydrogen. Fully substituted phosphazenes (**sas 5a**–**5d** and **sbs 6a**–**6d**) were prepared by the reaction of partly substituted phosphazenes (**sas 3** and **sbs 4**) with excess heterocyclic amines (pyrrolidine, piperidine, morpholine and DASD) in dry THF.

In the literature, only *spiro* phosphazenes were obtained from the reaction of $N_3P_3Cl_6$ with ethane-1,2-diamine [33], therefore **sas** (**3** and **5a**–**5d**) and **sbs** (**4** and **6a**–**6d**) are the first examples of the *ansa* and *bino* structures having ethane-1,2-diamine precursors, respectively. The P–N bonds of the seven membered *ansa* rings of **3**, **5a**, **5c** and **5d** have *cis* configuration according to the crystallographic data [34]. Analogously, the *cis* configuration is expected for **sas 5b**. The nucleophilic substitution reaction of K_2(**2**) with $N_3P_3Cl_6$ is of importance in providing tetra-substituted phosphorus atoms which are centers of chirality. As a result of the reaction, each **sas** compound (**3**, **5a**–**5d**) contains 2 equiv chiral P-atoms in seven membered *ansa* ring. Therefore, they have *R* and *S* configurations (*meso* form).

3.2. FTIR spectroscopy

The FTIR spectra of **sas** (**5b** and **5c**) and **sbs** (**6a**–**6d**) phosphazene derivatives display strong stretching bands at 1198–1180 cm^{-1} related to P=N bonds of the phosphazene rings. The aromatic C–H stretching bands are observed at around 3071–3030 cm^{-1}. The partly substituted **sas 3** and **sbs 4** give the stretching bands of PCl_2 bonds at 546 and 575 cm^{-1}, respectively. These bands disappear in the IR spectra of the fully heterocyclic amine substituted phosphazenes.

3.3. MS spectrometry

The fragments were observed under electrospray ionization (ESI-MS) (for **5b**, **6b** and **6d**) and atmospheric pressure ionization with electrospray (API–ES) (for **5c**, **6a** and **6c**) mass spectrometry conditions. The compounds (**5b**, **5c**, **6a** and **6c**) give protonated molecular ions $[MH]^+$ which are the parent or the second peaks in relative intensity. Notably, the MS spectra of **6a**–**6d** show [(hetereocyclic amine)$_4P_3N_3OArCH_2NCH_3]^+$ ions. These peaks are observed as parent peaks for **6b** and **6d**. In the unimolecular decomposition of the phosphazenes, the major fragmentation pathway involves the initial cleavage of the C–N bonds in the N–CH_2–CH_2–N precursor for **sbs** (**6a**–**6d**) and the exocyclic P–N bond with the loss of hetereocyclic amine groups for **sas** (**5a**, **5c** and **5d**).

3.4. NMR spectroscopy

The proton-decoupled ^{31}P NMR spectra of the fully substituted phosphazenes exhibit an AB_2 spin system containing two magnetically equiv ^{31}P NMR nuclei in the phosphazene rings, indicating the heterocyclic amine substituents replace all of the Cl-atoms in compounds **3** and **4** (Table 2). The ^{31}P NMR spectra of fully heterocyclic amine substituted **sas 5b** and **5c** do not show a typical five-line resonance pattern consisting of a *doublet* and a *triplet* and the δP shifts overlap centering at *ca.* 24 ppm. The ^{31}P NMR spectra of **6b**–**6d** give two sets of peaks around $\delta = 16$ and 22 ppm in a *doublet–triplet* pattern because of their **sbs** structures, which are assigned to the two OPN and four XPX phosphorus atoms. Whereas, the ^{31}P NMR spectrum of **6a** gives an $AB_2A'B'_2$ spin system, which is characterized by a small shift in the phosphorus-phosphorus coupling constants ($^2J_{PP}$).

The ^1H and ^{13}C NMR assignments of the compounds are summarized in Table 3. The interpretations are made unambiguously by HSQC and DEPT spectra. The HSQC spectrum of **5c** is depicted in Fig. 1, as an example. The aliphatic regions of the ^1H NMR spectra of the **sas** compounds are very complex since all of the aliphatic protons are diastereotopic. In the fully heterocyclic amine substituted derivatives (**5a**, **5b** and **5d**) and (**6a**, **6b** and **6d**), the NC***H***$_2$ proton signals of the heterocyclic amines are easily distinguished from those of the *ansa* and *bino* rings by the HSQC spectra of these compounds. The NC***H***$_2$ protons of **sas** (**3** and **5a**–**5d**) and **sbs** (**4** and **6a**–**6d**) give *multiplet* and *doublet* (*ca.* $^3J_{PH} = 11$ Hz) signals at $\delta = 3.12$–3.54 ppm, respectively. In the ^1H NMR spectra of **sas 5a**–**5d**, the two substituents bonded to the same P-atom show two groups of NC***H***$_2$ signals (3.12 and 3.27 ppm for **5a**, 3.14 and 3.20 ppm for **5b**, 3.21 and 3.25 ppm for **5c**, 3.32 and 3.38 ppm for **5d**) with small separations, indicating that the two geminal substituents are not equivalent to each other (Table 3, see a schematic representation of **sas-**structure). The ArC***H***$_2$ benzylic protons of **sas** derivatives are separated from each other at *ca.* 3.90 and 4.50 ppm as two peak groups. In addition, the ArC***H***$_2$ benzylic protons give rise to *doublet* with three bond coupling to the P-atom ($^3J_{PH}$) of *ca.* 15 Hz for **sbs** derivatives indicating that the ArC***H***$_2$ protons are equivalent. The four different proton signals of the aromatic rings for the phosphazene derivatives are two sets of *doublets* and *triplets*.

All of the expected carbon peaks are interpreted from the ^{13}C NMR spectra of the compounds. The most reliable evidence coming from the substitution of all the Cl-atoms of partly substituted **sas 3** and **sbs 4** phosphazenes is that the carbon signals of heterocyclic amine substituents are observed in the ^{13}C NMR spectra of the compounds. The values of the three-bond coupling constants $^3J_{PC}$ are observed for $NCH_2\boldsymbol{C}H_2$ carbons of **sas** (**5a** and **5b**) and **sbs** (**6a** and **6b**) phosphazenes ($^3J_{PC}$ *ca.* 8.2 Hz) and O***C***H_2 carbons of fully morpholine substituted derivatives (**5c** and **6c**) ($^3J_{PC}$ *ca.* 7.8 Hz). In addition, the values of the two-bond coupling constants, $^2J_{PC}$, are estimated at 3.1, 7.0 and 6.0 Hz for *bino*-bridge N***C***H_2 carbons of partly (**4**), and fully piperidine (**6b**) and morpholine (**6c**) substituted phosphazene derivatives. The couplings, $^2J_{PC1}$, $^3J_{PC2}$, and $^3J_{PC6}$, are observed as *triplets* for the **sas** phosphazenes and *doublets* for the **sbs** phosphazenes. The triplets observed for the **sas** phosphazenes may be due to the second-order effects which have previously been observed [35], and the J_{PC} coupling constants between the external transitions of the *triplets* are estimated. The peaks of non-protonated C atoms disappear in the DEPT spectra, as compared with the ^1H decoupled ^{13}C NMR spectra (Fig. 1S).

Table 2
^{31}P NMR Data ($CDCl_3$) of **3**, **4**, **5a**–**5d** and **6a**–**6d** (δ in ppm, J in Hz).

Compound	Spin system	δClPCl	δXPX	δOPN	$^2J_{PP}$
(**3**)	A_2X	P_X:29.35	–	P_A:19.59	$^2J_{AX}$:70.1
(**5a**)	AB_2	–	P_A:20.15	P_B:24.10	$^2J_{AB}$:53.5
(**5b**)	AB_2		~23.69		
(**5c**)	AB_2		~23.90		
(**5d**)	AB_2		~23.50		
(**4**)	AX_2	P_X:25.10	–	P_A:6.56	$^2J_{AX}$:56.1
(**6a**)	$AB_2A'B'_2$	–	P_B:18.98	P_A:17.47	$^2J_{AB}$:47.3
			$P_{B'}$:18.96	$P_{A'}$:17.42	$^2J_{A'B'}$:44.5
(**6b**)	AB_2	–	P_B:22.49	P_A:16.68	$^2J_{AB}$:46.0
(**6c**)	AB_2	–	P_B:21.62	P_A:16.53	$^2J_{AB}$:47.0
(**6d**)	AB_2	–	P_B:21.58	P_A:16.12	$^2J_{AB}$:47.3

3.5. X-ray crystallography

The molecular and solid state structures of **5c** and **6c** along with the atom-numbering schemes are depicted in Figs. 2 and 3, respectively. The asymmetric unit of **5c** contains one uncoordinated CH_3-CN and a phosphazene derivative containing a **sas** structure together with two morpholino substituents (Fig. 2S). The symmetric phosphazene derivative with a **sbs** structure and eight morpholino substituents contains 0.5 mol of **6c** and 1 mol of CH_3CN in its asymmetric unit (Fig. 3S). As can be seen from the packing diagrams of **5c** and **6c**, the CH_3CN molecules occupy the cavities [36]. Dipole–dipole and van der Waals interactions are effective in the molecular packing. There are intra- and intermolecular C–H···N hydrogen bonds in **5c**, while **6c** has intramolecular C–H···N and intermolecular C–H···O hydrogen bonds (Table 2S). The findings in the IR spectra of **5c** and **6c** ($\nu_{CH\cdots N}$ stretching band for **5c** at 3442 cm^{-1} and $\nu_{CH\cdots N}$ and $\nu_{CH\cdots O}$ stretching bands for **6c** at 3446 cm^{-1}) support X-ray crystallographic data.

The phosphazene rings of **5c** and **6c** are in twisted and flattened-boat conformations, respectively [Fig. 4Sa; $\varphi_2 = 90.4(2)^\circ$, $\theta_2 = 53.5(2)^\circ$ (P1/N1/P2/N2/P3/N3) (for **5c**) and Fig. 5Sa; $\varphi_2 = -168.3(8)^\circ$, $\theta_2 = 110.7(8)^\circ$6 (for **6c**)] having total puckering amplitudes [37], Q_T, of 0.421(2) Å for **5c** and Q_T of 0.170(3) Å for **6c**. In **5c**, the seven-membered *ansa* ring (N1/P1/N6/C23/C24/N7/P2) and the six-membered *spiro* rings (P1/N6/C9/C10/C15/O3) and (P2/N7/C16/C17/C22/O4) are in twisted, boat and twisted conformations, respectively [Fig. 4Sb; $Q_T = 1.133(3)$ Å, $\varphi_2 = 98.9(4)^\circ$, $\theta_2 = 12.0(1)^\circ$ (N1/P1/N6/C23/C24/N7/P2), $Q_T = 0.552(2)$ Å, $\varphi_2 = 162.9(3)^\circ$, $\theta_2 = 92.7(3)^\circ$ (P1/N6/C9/C10/C15/O3), $Q_T = 2.478(2)$ Å, $\varphi_2 = 148.1(3)^\circ$, $\theta_2 = 21.1(1)^\circ$ (P2/N7/C16/C17/C22/O4)]. In **6c**, the

Table 3
^{1}H and ^{13}C NMR Data ($CDCl_3$) of **3**, **4**, **5a–5d** and **6a–6d** (δ in ppm, *J* in Hz, s: *singlet*, d: *doublet*, t: *triplet*, q: *quartet* and m: *multiplet* peak).

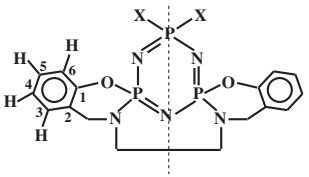

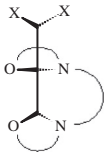

Schemetic representative structure of **sas**

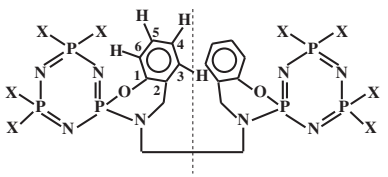

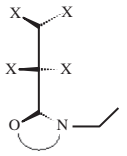

Schemetic representative structure of **sbs**

		(**3**)	(**5a**)	(**5b**)	(**5c**)	(**5d**)	(**4**)	(**6a**)	(**6b**)	(**6c**)	(**6d**)
H											
$NCH_2CH_2C\boldsymbol{H}_2$		–	–	1.67 (m,4H)	–	–	–	–	1.67 (m,16H)	–	–
$NCH_2C\boldsymbol{H}_2$		–	1.86 (m,8H)	1.59 (m,8H)	–	1.62 (m,2H) 1.77 (m,6H)	–	3.32 (m,32H)	1.53 (m,32H)	–	1.67 (m,32H)
$NC\boldsymbol{H}_2$			*pyrrolidine* 3.23 (m,4H) 3.27 (m,4H)	*piperidine* 3.13 (m,4H) 3.20 (m,4H)	*morpholine* 3.21 (m,4H) 3.25 (m,4H)	*DASD* 3.32 (m,4H) 3.38 (m,4H)		*pyrrolidine* 3.17 (m,32H)	*piperidine* 3.09 (m,32H)	*morpholine* 3.10 (m,32H)	*DASD* 3.21 (m,32H)
		ansa 3.30 (m,2H) 3.54 (m,2H)	*ansa* 3.12 (m,2H) 3.43 (m,2H)	*ansa* 3.14 (m,2H) 3.44 (m,2H)	*ansa* 3.14 (m,2H) 3.45 (m,2H)	*ansa* 3.15 (m,2H) 3.44 (m,2H)	*bino* 3.34 (d,4H) $^{3}J_{PH}$ = 14.0	*bino* 3.32 (d,4H) $^{3}J_{PH}$ = 10.6	*bino* 3.31 (d,4H) $^{3}J_{PH}$ = 10.4	*bino* 3.28 (d,4H) $^{3}J_{PH}$ = 9.9	*bino* 3.26 (d,4H) $^{3}J_{PH}$ = 10.0
$OC\boldsymbol{H}_2$		–	–	–	3.71 (m,8H)	3.99 (s,4H) 4.00 (s,4H)	–	–	–	3.66 (m,32H)	3.93 (s,16H) 3.96 (s,16H)
$ArC\boldsymbol{H}_2N$		3.94 (m,2H) $^{3}J_{PH}$ = 15.0 4.56 (m,2H) $^{3}J_{PH}$ = 15.1	3.84 (d,2H) $^{3}J_{PH}$ = 15.0 4.47 (d,2H) $^{3}J_{PH}$ = 15.0	3.85 (q,2H) 4.49 (d,2H) $^{3}J_{PH}$ = 16.3	3.84 (q,2H) $^{2}J_{HH}$ = 15.0 $^{3}J_{PH}$ = 11.0 4.47 (d,2H) $^{2}J_{HH}$ = 15.0 $^{3}J_{PH}$ = 10.2	3.84 (q,2H) 4.48 (d,2H) $^{3}J_{PH}$ = 14.8	4.38 (d,4H) $^{3}J_{PH}$ = 15.5	4.33 (d,4H) $^{3}J_{PH}$ = 14.3	4.37 (d,4H) $^{3}J_{PH}$ = 14.8	4.38 (d,4H) $^{3}J_{PH}$ = 14.4	4.35 (d,4H) $^{3}J_{PH}$ = 14.4
$Ar\boldsymbol{H}$	$\boldsymbol{H}_3$	7.09–7.29	7.03 (d,2H)	7.05 (d,2H)	7.04 (d,2H)	7.02 (d,2H)	6.96–7.09	6.94–6.84	6.90–6.86	7.09–6.96	6.87–7.09
	$\boldsymbol{H}_4$	7.09–7.29	7.00 (t,2H)	7.00 (t,2H)	7.01 (t,2H)	6.96 (t,2H)	6.96–7.09	6.94–6.84	6.91 (t,2H)	7.09–6.96	6.87–7.09
	$\boldsymbol{H}_5$	7.09–7.29	7.18 (t,2H)	7.20 (t,2H)	7.21 (t,2H)	7.16 (t,2H)	7.28 (t,2H)	7.13 (t,2H)	7.14 (t,2H)	7.19 (t,2H)	7.12 (t,2H)
	$\boldsymbol{H}_6$	7.09–7.29	7.02 (d,2H)	7.03 (d,2H)	7.03 (d,2H)	7.01 (d,2H)	6.96–7.09	6.94–6.84	6.90–6.86	6.88 (d,2H)	6.87–7.09
$^{3}J_{3-4}$		*	8.4	8.7	8.7	8.5				*	*
$^{3}J_{4-5}$		*	7.3	7.7	7.6	7.3				7.6	*
$^{3}J_{5-6}$		*	8.0	8.2	8.5	8.1				7.9	*
C											
$NCH_2CH_2\boldsymbol{C}H_2$		–	–	25.0 25.1	–	–	–	–	25.0 25.2	–	–
$NCH_2\boldsymbol{C}H_2$		–	26.3 $^{3}J_{PC}$ = 6.3 26.4 $^{3}J_{PC}$ = 5.9	26.2 $^{3}J_{PC}$ = 5.9 26.4 $^{3}J_{PC}$ = 7.1	–	35.3 $^{3}J_{PC}$ = 5.7 35.6 $^{3}J_{PC}$ = 4.9	–	26.36 $^{3}J_{PC}$ = 9.3 26.37 $^{3}J_{PC}$ = 8.7	26.3 $^{3}J_{PC}$ = 7.9 26.4 $^{3}J_{PC}$ = 8.0		35.76 35.82
NCH_2			*pyrrolidine* 46.1 $^{2}J_{PC}$ = 3.8 46.3 $^{2}J_{PC}$ = 4.0	*piperidine* 45.1 45.2	*morpholine* 42.8 42.7	*DASD* 42.6 42.8		*pyrrolidine* 46.0 46.2	*piperidine* 45.3 45.4	*morpholine* 44.6 42.7	*DASD* 42.8 42.9
		ansa 52.0	*ansa* 53.6	*ansa* 51.5	*ansa* 51.7	*ansa* 53.5	*bino* 47.3 $^{2}J_{PC}$ = 3.1	*bino* 47.6	*bino* 47.6 $^{2}J_{PC}$ = 7.0	*bino* 47.1 $^{2}J_{PC}$ = 6.0	*bino* 46.9
OCH_2		–	–	–	65.4 $^{3}J_{PC}$ = 6.6 65.2 $^{3}J_{PC}$ = 6.7	64.2 64.3	–	–	–	67.14 $^{3}J_{PC}$ = 8.5 67.18 $^{3}J_{PC}$ = 8.1	64.4
OCO		–	–	–	–	107.6	–	–	–	–	107.7

(*continued on next page*)

Table 3 (*continued*)

H	(3)	Schemetic representative structure of **sas** (5a)	(5b)	(5c)	(5d)	Schemetic representative structure of **sbs** (4)	(6a)	(6b)	(6c)	(6d)
$ArCH_2N$	53.7	51.6	53.4	49.7	51.6	50.2 $^2J_{PC}$ = 1.8	49.8	50.0	49.8	108.0 49.7
ArC C_1	150.5 $^2J_{PC}$ = 6.2	151.2 $^2J_{PC}$ = 6.1	151.2 $^2J_{PC}$ = 5.0	149.1	151.1	150.2 $^2J_{PC}$ = 8.4	152.0 $^2J_{PC}$ = 8.0	151.9 $^2J_{PC}$ = 8.5	151.1	151.7 $^2J_{PC}$ = 8.6
C_2	124.1 $^3J_{PC}$ = 8.3	124.8 $^3J_{PC}$ = 8.1	124.8 $^3J_{PC}$ = 7.5	122.6 $^3J_{PC}$ = 7.3	124.6	124.5 $^3J_{PC}$ = 7.0	124.7 $^3J_{PC}$ = 7.4	124.7 $^3J_{PC}$ = 7.5	123.7 $^3J_{PC}$ = 8.0	125.0 $^3J_{PC}$ = 7.7
C_3	127.0	126.4	126.3	124.6	126.4	127.0	126.3	126.4	126.7	127.0
C_4	124.5	123.0	123.0	121.5	123.2	123.0	121.9	123.0	122.9	122.5
C_5	129.4	128.4	128.4	126.8	128.5	128.4	128.2	127.8	128.4	128.1
C_6	119.6 $^3J_{PC}$ = 9.2	119.0 $^3J_{PC}$ = 8.6	118.9 $^3J_{PC}$ = 9.0	117.1 $^3J_{PC}$ = 7.5	119.1	119.0 $^3J_{PC}$ = 8.2	119.0 $^3J_{PC}$ = 7.5	118.3 $^3J_{PC}$ = 7.5	118.3 $^3J_{PC}$ = 7.6	118.7 $^3J_{PC}$ = 6.9

* Not calculated.

six-membered ring (P1/O1/C1/C6/C7/N4) is in twisted form [Fig. 5Sb; Q_T = 0.527(3) Å, φ_2 = 123.5(5)°, θ_2 = 91.3(5)°]. The bicyclic system made up of phosphazene and *ansa* rings of **5c** is in a sofa conformation (Fig. 4Sc). Each ring is V-shaped, with the nonplanar two halves (P2/N2/P3/N3/P1) and (P1/N6/C23/C24/N7/P2). The sums of the bond angles around the atoms N6 and N7 [345.1(2)° and 347.6(2)°] show changes in hybridizations of the atoms from trigonal planar towards a pyramidal for **5c** [38]. The distortions of the N-atoms especially may depend on the conformations of phosphazene and *spiro* rings (Fig. 4Sb). Since the compounds (**5a**–**5d**) are fluxional in solution, the distortion may also be purely caused by packing effects in the solid state.

The average endocyclic PN bond lengths of **5c** and **6c** are 1.591(2) Å (for **5c**) and 1.588(3) Å (for **6c**), respectively, which are considerably shorter than the average exocyclic PN bonds [1.636(2) Å for **5c** and 1.644(3) Å for **6c**], indicating that the endocyclic PN bonds have double bond character. The value of the endocyclic P1N1P2 angle of **5c** [112.8(1)°] is highly smaller than those of P2N2P3 [117.4(1)°] and P1N3P3 [122.8(1)°], and the corresponding value of the starting dichloro **sas 3** [114.1(3)°] [39]. The endocyclic NPN angles of **5c** and **6c** are considerably narrowed with respect to the corresponding value in the "standard" compound $N_3P_3Cl_6$ [118.3(2)°]. Moreover, all the endocyclic PNP angles of **5c** are noticeably narrowed, except P1N3P3 angle but, the endocyclic PNP angles of **6c** are slightly expanded with respect to corresponding value of $N_3P_3Cl_6$ [121.4(3)°] [40].

3.6. The relationship between ^{31}P NMR spectroscopy and X-ray crystallography

A number of relationships gained from ^{31}P NMR spectra and X-ray crystallographic results is observed using the exocyclic OPN bond angles (α′) and the bond lengths (a, a′, b and b′) of the phosphazene rings (Scheme 2, Table 4). These include (i) α′ versus δP_{OPN} shifts (Fig. 4A) and (ii) the electron density transfer parameters Δ(P–N) [Δ(a–b): the difference between the bond lengths of two adjacent P–N bonds] and their relationships with both Δ(δP) and δP_{OPN} shifts (Fig. 4B). The variations in the bond angles and δP-shifts of the phosphazenes depend on the electronic and steric factors. It is found that relatively small changes in α′ bond angles are shown to cause large changes in δP_{OPN} shifts according to Fig. 4A. Moreover, the correlations between δP_{OPN} shifts and α′ bond angles for the fully heterocyclic amine (Fig. 4Aa) and partly (Fig. 4Ab) substituted **sas**, **sbs** and *spiro* [41–45] phosphazene derivatives show contrasting trends. On the other hand, Δ(P–N) indicates the measure of the electron releasing and withdrawing capacities of the substituents bonded to phosphazene ring [46] and the Δ(P–N) values are calculated from the equations given in Scheme 2. When the substituents bonding to the phosphazene ring withdraw electrons from the phosphazene ring, Δ(P–N) values are getting increases. In addition, the shortening of the exocyclic P–N bonds is to be a measure of the electron withdrawing capacities of the substituents, hence, which is likely to be a measure of the negative hyperconjugation. The electron releasing capacities of the substituents for **3**, **5a**, **5c** and **5d** are in the following order: DASD > pyrrolidine > morpholine > Cl. A similar situation is observed for partly (**I**) and fully morpholino (**6c**) substituted **sbs** compounds. The homologous partly and fully heterocyclic amine substituted *spiro*-phosphazenes given in Scheme 2 can also be compared with each other in Fig. 4. Based on the electron releasing capacities of the morpholine substituents in the **sas 5c** and **sbs 6c** skeletons, the electrons are slightly transferred from morpholine groups to the phopsphazene ring in **5c**.

Consequently, the origin of the PN bonds in the cyclophosphazene derivatives is still not clearly understood. A number of attempts have been made to explain the origin of the PN bonds

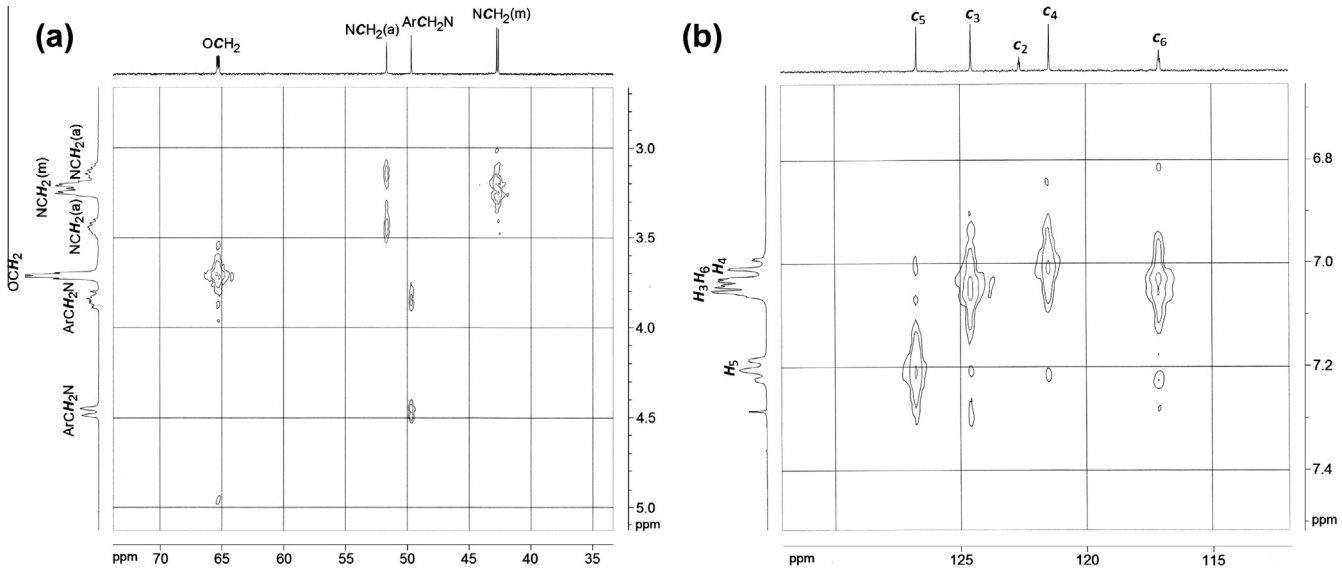

Fig. 1. HSQC spectrum (a) for the aliphatic region and (b) aromatic region of **5c** (a:*ansa*, m:morpholine).

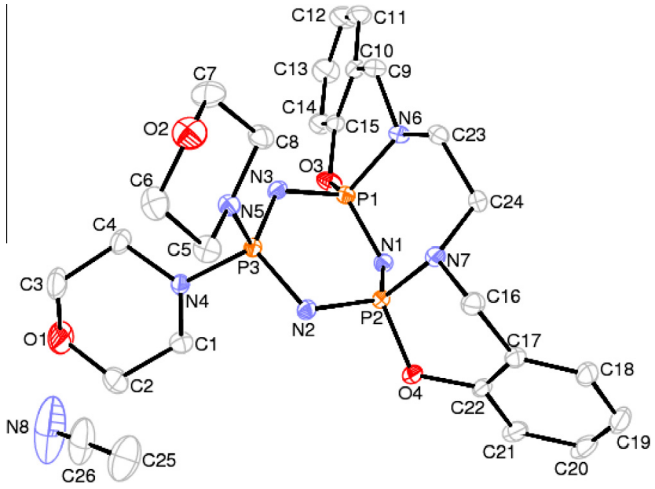

Fig. 2. ORTEP-3 drawing of **5c** with the atom-numbering scheme. Displacement ellipsoids are drawn at the 30% probability level.

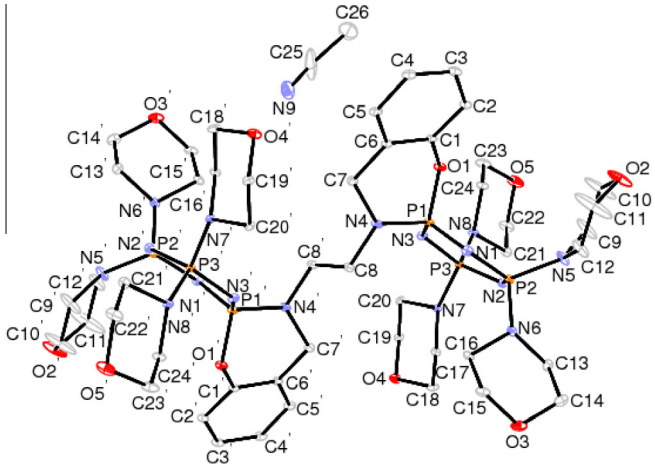

Fig. 3. ORTEP-3 drawing of **6c** with the atom-numbering scheme. Displacement ellipsoids are drawn at the 30% probability level.

using the island [47] and the negative hyperconjugation models [48]. In the negative hyperconjugation model, which is the newest one, the electronic structures and the PN bonds of phosphazenes are investigated using natural bond orbital (NBO) and topological electron density analyses. The ionic bonding and negative hyperconjugation alternatives for phosphazene derivatives are mutually exclusive. While the electron releasing groups bonding to the P-atoms decrease the negative hyperconjugation of the PN bonds, the electron withdrawing groups increase the multiple-bond character of the PN bonds. Therefore, the narrowing and broadening of the endocyclic NPN and PNP angles, and the shortening of the PN bonds of the phosphazenes may significantly depend on the conformation and electron releasing and withdrawing capacities of the substituents, the steric hindrances of the exocyclic groups, the *spiro* rings bonded to the P-atoms and the negative hyperconjugation.

3.7. Antimicrobial activity

The starting compound ($N_3P_3Cl_6$), pyrrolidine, piperidine, morpholine, DASD and dibenzo-diaza podand (**2**) were subjected to antimicrobial activity against the bacteria and yeast strains tested for phosphazene derivatives (**3**, **4**, **5a**–**5d** and **6a**–**6d**) in this study. $N_3P_3Cl_6$ exhibits weak antibacterial activity against *B. subtilis* ATCC 6633 (G+), *B. cereus* NRRL-B-3711 (G+) and *E. coli* ATCC 25922 (G−), piperidine to *B. cereus* NRRL-B-3711 (G+), morpholine to *P. aeruginosa* ATCC 27853 (G−), and DASD to *B. subtilis* ATCC 6633 (G+) and *B. cereus* NRRL-B-3711 (G+). The results were given in Table 3S for comparison to the cyclotriphosphazene derivatives. Phosphazene derivatives **3**, **4**, **5a**–**5d** and **6a**–**6d** exhibit no antibacterial activity even if they have been used at 5000 μM. The hetereocyclic amines and starting compounds do not show antifungal activity. However, compound **6a** displays good activity (15.0 ± 0.0) against yeast strain *C. tropicalis* compared with that of Ketoconazole (29.0 ± 0.0) (Table 3S). The activity for **6a** may be attributed to the presence of both the **sbs** architecture and pyrrolidinyl side groups.

3.8. Interactions of DNA with the compounds

The interactions of $N_3P_3Cl_6$, pyrrolidine, piperidine, morpholine, DASD, **2** and cyclotriphosphazene derivatives (**3**, **4**, **5a**–**5d** and

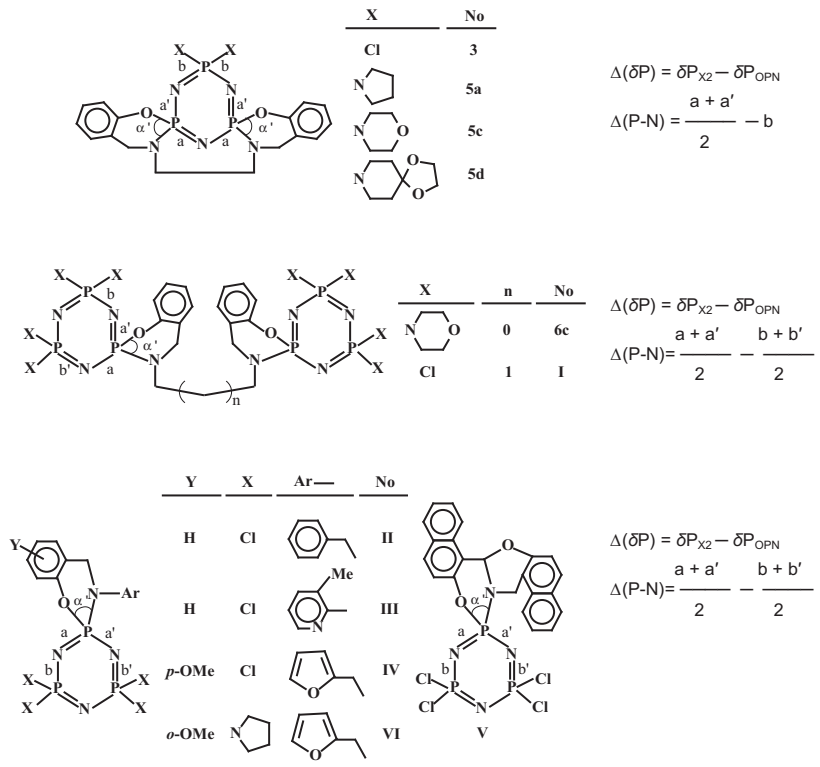

Scheme 2. The exocyclic OPN bond angles (α′) and bond lengths (a, a′, b and b′) on the formulae of the **sas**, **sbs** and *spiro*-phosphazenes.

Table 4
Exoxcyclic OPN bond angles (α′), bond lengths (a, a′, b and b′), δP–shifts, Δ(P–N) and Δ(δP) values for the compounds [δP in ppm, α′ angles in (°)].

Compound	(**a**)	(**a′**)	(**b**)	(**b′**)	Δ(P–N)	(**α′**)	δP_{OPN}	δP_{X2}	Δ(δP)
(**3**)	1.588(5)	1.602(5)	1.564(5)	–	0.0310	104.0(3)	19.59	29.35	9.76
	1.579(5)	1.621(6)	1.621(6)	–	−0.0210	104.4(2)			
(**5a**)	1.589(3)	1.577(3)	1.697(3)	–	−0.0260	101.55(16)	20.15	24.10	3.95
	1.584(3)	1.567(3)	1.600(3)	–	−0.0245	104.44(15)			
(**5c**)	1.5811(18)	1.5890(19)	1.6059(18)	–	−0.0209	101.33(9)	23.9	24.2	0.30
	1.5888(19)	1.5775(19)	1.6037(18)	–	−0.0206	105.17(9)			
(**5d**)	1.590(5)	1.586(4)	1.595(5)	–	−0.0700	102.2(2)	23.25	23.50	0.25
	1.577(5)	1.585(4)	1.604(4)	–	−0.0230	102.6(2)			
(**6c**)	1.584(3)	1.571(4)	1.601(4)	1.600(3)	−0.0230	100.96(16)	16.53	21.62	5.09
(I)	1.594(5)	1.589(5)	1.563(5)	1.573(6)	0.0235	103.81(17)	6.78	25.09	18.31
	1.575(5)	1.582(6)	1.566(5)	1.554(6)	0.0185	102.65(15)			
(II)	1.600(3)	1.583(3)	1.563(3)	1.569(3)	0.0255	102.97(13)	3.90	24.73	20.83
(III)	1.589(4)	1.597(4)	1.569(3)	1.564(3)	0.0265	100.3	5.15	26.32	21.17
(IV)	1.594(2)	1.604(2)	1.567(2)	1.557(2)	0.0370	102.7(1)	5.25	23.87	18.62
(V)	1.592(3)	1.607(3)	1.563(3)	1.554(3)	0.0410	101.03	1.60	24.5 26.7	24.00
(VI)	1.577(2)	1.583(2)	1.606(2)	1.600(2)	−0.023	100.5(1)	17.88	19.36	1.48

6a–**6d**) with supercoiled pBR322 DNA were investigated using the agarose gel electrophoresis. Fig. 5 gives the electrophoretograms applying to have incubated mixtures of pBR322 plasmid DNA and varying concentrations (5000–625 μM) of the compounds. Lane P applies to the untreated pBR322 plasmid DNA (control DNA), showing the major supercoiled circular form I and minor singly nicked relaxed circular form II of the plasmid DNA. Lanes 1–4 apply to pBR322 plasmid DNA incubated with the compounds ranging from 5000 to 625 μM. Pyrrolidine, morpholine and **2** have no effect on plasmid DNA. Piperidine and DASD cause only a very small decrease in the mobility of form I DNA. However, $N_3P_3Cl_6$ causes significant conformational change.

The phosphazene derivatives **5d**, **6b** and **6c** cause a decrease in the mobility and intensity of form I DNA, whereas that of the form II band remains essentially unchanged. When pBR322 plasmid DNA is interacted with **5b** and **5c**, there is a slight decrease in intensity of form I, and the mobility and intensity of form II remain unchanged. In case of **5a**, **6a** and **6d**, there is a slight decrease in mobility of form I at two higher concentrations. The linear band is also observed for **6a** in addition to decrease in mobility. The partly substituted phosphazene derivatives (**3** and **4**) are found to be more damaging to DNA. Compounds **3** and **4** increase in mobility and intensity of form II DNA. The ClPCl angle of partly substituted **sas 3** phosphazene (99.6°) is close to the ClPtCl angle

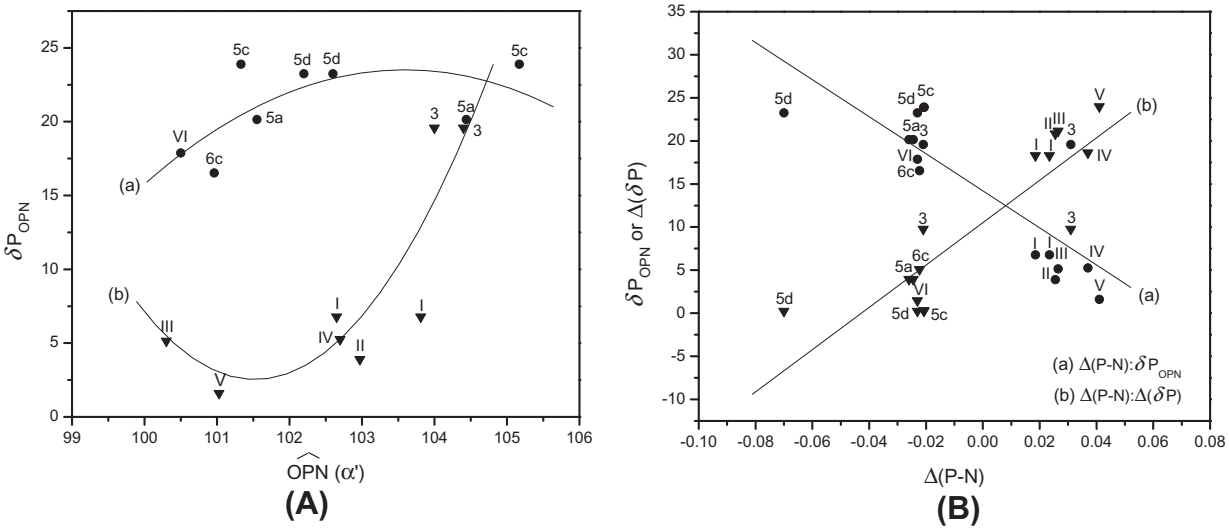

Fig. 4. The relationship between (A) exocyclic OPN bond angles (α') and δP_{OPN} shifts for (a) the fully heterocyclic amine and (b) partly substituted **sas**, **sbs** and *spiro*-phosphazenes and (B) (a) Δ(P–N) and δP_{OPN} shifts and (b) Δ(P–N) and Δ(δP) values for the partly and fully heterocyclic amine substituted **sas**, **sbs** and *spiro*-phosphazenes.

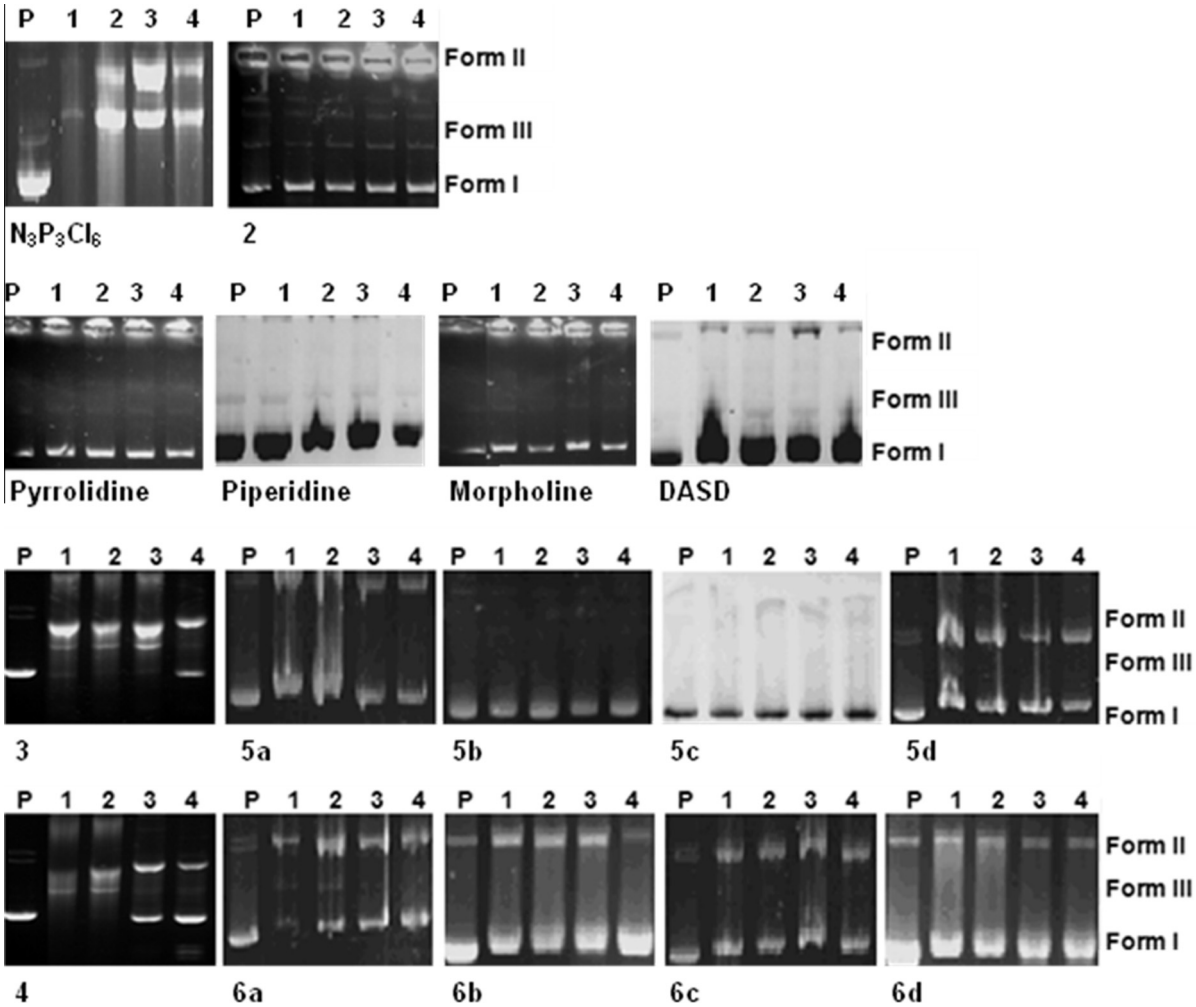

Fig. 5. Gel electrophoretic mobility of pBR322 plasmid DNA, when incubated with different concentrations of $N_3P_3Cl_6$, pyrrolidine, piperidine, morpholine, DASD, **2**–**4**, **5a**–**5d** and **6a**–**6d**. Lane P applies untreated pBR322 plasmid DNA. Concentrations (in μM) are as follows: lanes 1 to 4 apply to plasmid DNA interacted with decreasing concentrations of the compounds: lane 1: 5000; lane 2: 2500; lane 3 1250; lane 4: 625. The top and the bottom bands correspond to form II (single nicked open circular), form I (covalently closed circular or supercoiled) and form III (linear) plasmids, respectively.

of *cis*-platin (92°) [49]. Thus, the interactions of **3** and *cis*-platin with DNA are likely to be considered similar.

4. Conclusions

The syntheses and characterizations of fully heterocyclic amine substituted **sas 5a–5b** and **sbs 6a–6b** phosphazenes were described. The partly substituted **sas 3** and **sbs 4** phosphazenes reacted with excess heterocyclic amines in THF to produce the fully substituted **sas 5a–5d** and **sbs 6a–6d** phosphazenes, respectively. All the compounds were characterized by one and two dimensional NMR techniques, where the fully morpholine substituted **sas 5c** and **sbs 6c** phosphazenes were characterized crystallographically. In **sas** compounds, there are two stereogenic P-atoms. They have *meso* form. Compound **6a** is active against yeast strain *C. tropicalis*. Interactions between the phosphazenes and pBR322 plasmid DNA show that the partly substituted **sas 3** and **sbs 4** phosphazenes are effective in changing the mobility and intensity of form II DNA.

Acknowledgements

The authors would like to express their deep sense of gratitude and heartiest thanks to Ankara University Scientific Research Projects (BAP) (Grant No. 10B4240008), Hacettepe University Scientific Research Unit (Grant No. 02 02 602 002) and State Planing Organization (grant No.1998K121480) for financial support of this work.

Appendix A. Supplementary material

The crystal packing diagrams, ring conformations and hydrogen-bond geometries for **sas** (**5c**) and **sbs** (**6c**) phosphazenes, and antimicrobial activities of $N_3P_3Cl_6$ and heterocyclic amines. CCDC 917208 and 917209 contains the supplementary crystallographic data for these compounds **5c** and **6c**. These data can be obtained free of charge from The Cambridge Crystallographic Data Centre via www.ccdc.cam.ac.uk/data_request/cif. Supplementary data associated with this article can be found, in the online version, at http://dx.doi.org/10.1016/j.ica.2013.07.023.

References

[1] C.W. Allen, in: R. Steudel (Ed.), Studies in Inorganic Chemistry, Elsevier Science Publishers B.V., 1992, pp. 171–191.
[2] M. Gleria, R. De Jaeger, Phosphazenes: A Worldwide Insight, Nova Science Publishers Inc., 2004.
[3] B.A. Omotowa, B.S. Phillips, J.S. Zabinski, J.M. Shreeve, Inorg. Chem. 43 (2004) 5466.
[4] J. Jiménez, A. Laguna, E. Gascón, J.A. Sanz, J.L. Serreno, J. Barberá, L. Oriol, Chem. Eur. J. 18 (2012) 16801.
[5] L.-J. Qian, L.-J. Ye, G.-W. Xu, J. Liu, J.-Q. Guo, Polym. Degrad. Stabil. 96 (2011) 1118.
[6] P. Schroögel, M. Hoping, W. Kowalsky, A. Hunze, G. Wagenblast, C. Lennartz, P. Strohriegl, Chem. Mater. 23 (2011) 4947.
[7] S.V. Sazhin, M.K. Harrup, K.L. Gering, J. Power Sources 196 (2011) 3433.
[8] S. Bilge Koçak, Turk. J. Chem. 35 (2011) 745.
[9] R.K. Voznicová, J. Taraba, J. Příhoda, M. Alberti, Polyhedron 27 (2008) 2077.
[10] I. Porwolik-Czomperlic, K. Brandt, T.A. Clayton, D.B. Davies, R.J. Eaton, R.A. Shaw, Inorg. Chem. 41 (2002) 4944.
[11] S. Beşli, S.J. Coles, D.B. Davies, R.J. Eaton, M.B. Hursthouse, A. Kılıç, R.A. Shaw, G.Y. Çiftçi, S. Yeşilot, J. Am. Chem. Soc. 125 (2003) 4943.
[12] S. Sengupta, Polyhedron 22 (2003) 1237.
[13] K. Brandt, I. Porwolic-Czomperlik, M. Siwy, T. Kupka, R.A. Shaw, S. Ture, A. Clayton, D.B. Davies, M.B. Hursthouse, G.D. Sykara, J. Org. Chem. 64 (1999) 7299.
[14] M.A. Benson, R. Boomishankar, D.S. Wright, A. Steiner, J. Organomet. Chem. 692 (2007) 2768.
[15] M. Yıldız, Z. Kılıç, T. Hökelek, J. Mol. Struct. 510 (1999) 227.
[16] D. Kumar, N. Singh, K. Keshav, A.J. Elias, Inorg. Chem. 50 (2011) 250.
[17] S.J. Coles, D.B. Davies, R.J. Eaton, M.B. Hursthouse, A. Kılıç, R.A. Shaw, A. Uslu, Dalton Trans. 10 (2006) 1302.
[18] S. Begeç, Heteroatom Chem. 18 (2007) 372.
[19] K. Muralidharan, A.J. Elias, Inorg. Chem. 42 (2003) 7535.
[20] K. Brandt, R. Kruszynski, T. Bartczak, I. Porwolik-Czomperlic, Inorg. Chim. Acta 322 (2001) 138.
[21] E.E. İlter, N. Asmafiliz, Z. Kılıç, L. Açık, M. Yavuz, E.B. Bali, A.O. Solak, F. Büyükkaya, H. Dal, T. Hökelek, Polyhedron 29 (2010) 2933.
[22] N. Asmafiliz, Z. Kılıç, A. Öztürk, T. Hökelek, L.Y. Koç, L. Açık, Ö. Kısa, A. Albay, Z. Üstündağ, A.O. Solak, Inorg. Chem. 48 (2009) 10102.
[23] L.J. Farrugia, J. Appl. Crystallogr. 30 (1997) 565.
[24] International Tables for X-Ray Crystallography, vol. IV, Kynoch Press, Birmingham, 1974 (Present Distributor: Kluwer Academic Publisher, Dordrecht, The Netherlands).
[25] A.C.T. North, D.C. Phillips, F.S. Mathews, Acta Crystallogr., Sect. A 24 (1968) 351.
[26] Bruker, SADABS, Bruker AXS Inc, Madison, Wisconsin, USA, 2005.
[27] G.M. Sheldrick, SHELXS-97 and SHELXL-97, University of Göttingen, Germeny, 1997.
[28] C. Perez, M. Paul, P. Bazerque, Acta. Biol. Med. Exp. 15 (1990) 113.
[29] A. Okumuş, Z. Kılıç, T. Hökelek, H. Dal, L. Açık, Y. Öner, L.Y. Koç, Polyhedron 30 (2011) 2896.
[30] A. Natsagdorj, Ph.D. Thesis, 2002, Ankara University, Department of Chemistry.
[31] S. Bilge, A. Natsagdorj, Ş. Demiriz, N. Çaylak, Z. Kılıç, T. Hökelek, Helv. Chim. Acta 87 (2004) 2088.
[32] S. Bilge, Ş. Demiriz, A. Okumuş, Z. Kılıç, B. Tercan, T. Hökelek, O. Büyükgüngör, Inorg. Chem. 45 (2006) 8755.
[33] M. Willson, L. Lafaille, L. Vidaud, J.F. Labarre, Phosphorus Sulfur 29 (1987) 147.
[34] B. Tercan, T. Hökelek, O. Büyükgüngör, S. Bilge, A. Okumuş, Z. Kılıç, Anal. Sci. 23 (2007) 121.
[35] S. Bilge, B. Özgüç, S. Safran, Ş. Demiriz, H. İşler, M. Hayvalı, Z. Kılıç, T. Hökelek, J. Mol. Struct. 748 (2005) 101.
[36] S. Bilge, S.J. Coles, D.B. Davies, M.B. Hursthouse, Z. Kılıç, J.S. Rutherford, R.A. Shaw, Cryst. Eng. Comm. 10 (2008) 873.
[37] D. Cremer, J.A. Pople, J. Am. Chem. Soc. 97 (1975) 1354.
[38] Z. Kılıç, A. Okumuş, Ş. Demiriz, S. Bilge, A. Öztürk, N. Çaylak, T. Hökelek, J. Incl. Phenom. Macrocycl. Chem. 65 (2009) 269.
[39] B. Tercan, T. Hökelek, S. Bilge, A. Natsagdorj, Ş. Demiriz, Z. Kılıç, Acta Crystallogr., Sect. E 60 (2004) o795.
[40] G.J. Bullen, J. Chem. Soc. A. (1971) 1450.
[41] N. Asmafiliz, Z. Kılıç, Z. Hayvalı, L. Açık, T. Hökelek, H. Dal, Spectrochim. Acta A 86 (2012) 214.
[42] M. Işıklan, Ö. Sonkaya, B. Coşut, S. Yeşilot, T. Hökelek, Polyhedron 29 (2010) 1612.
[43] H. Dal, S. Safran, Y. Süzen, T. Hökelek, Z. Kılıç, J. Mol. Struct. 753 (2005) 84.
[44] E.E. İlter, N. Çaylak, M. Işıklan, N. Asmafiliz, Z. Kılıç, T. Hökelek, J. Mol. Struct. 697 (2004) 119.
[45] B. Tercan, T. Hökelek, M. Işıklan, E.E. İlter, Z. Kılıç, Acta Crystallogr., Sect. E 60 (2004) 971.
[46] S. Beşli, S.J. Coles, D.B. Davies, M.B. Hursthouse, A. Kılıç, T. Mayer, R.A. Shaw, Acta Crystallogr., Sect. B 58 (2002) 1067.
[47] V.L. Minkin, R.M. Minyaev, Chem. Rev. 101 (2001) 1247.
[48] A.B. Chaplin, J.A. Harrison, P.J. Dyson, Inorg. Chem. 44 (2005) 8407.
[49] G.L. Miessler, D.A. Tarr, Inorg. Chem., second ed., Nortfield, Minnesota, 1999.